Identification of a novel subset of alveolar type 2 cells enriched in PD-L1 and expanded following pneumonectomy

Negah Ahmadvand[1,2], Farhad Khosravi [3], Arun Lingampally[1,2], Roxana Wasnick[2], Ana Ivonne Vazquez-Armendariz [2], Gianni Carraro[4], Monika Heiner[2], Stefano Rivetti[1,2], Yuqing Lv[1], Jochen Wilhelm[5], Andreas Gunther [2], Susanne Herold[2], Denise Al Alam [6], Chengshui Chen[1], Parviz Minoo[6,7], Jin-San Zhang[1,8] and Saverio Bellusci[1,2,8]

[1]Key Laboratory of Interventional Pulmonology of Zhejiang Province, Dept of Pulmonary and Critical Care Medicine, The First Affiliated Hospital of Wenzhou Medical University, Wenzhou, China. [2]Cardio-Pulmonary Institute, Institute of Lung Health and Dept of Pulmonary and Critical Care Medicine and Infectious Diseases, Universities of Giessen and Marburg Lung Center (UGMLC), member of the German Center for Lung Research (DZL), Justus-Liebig University Giessen, Giessen, Germany. [3]Dept of Physiology, Justus-Liebig University Giessen, Giessen, Germany. [4]Dept of Medicine, Cedars-Sinai Medical Center, Lung and Regenerative Medicine Institutes, Los Angeles, CA, USA. [5]Cardio-Pulmonary Institute (CPI), Universities of Giessen and Marburg Lung Center (UGMLC), Institute for Lung Health (ILH), Member of the German Center for Lung Research (DZL), Justus-Liebig University Giessen, Giessen, Germany. [6]Lundquist Institute for Biomedical Innovation at Harbor-UCLA Medical Center, Los Angeles, CA, USA. [7]Division of Newborn Medicine, Dept of Pediatrics, University of Southern California and Children's Hospital Los Angeles, Los Angeles, CA, USA. [8]J-S. Zhang and S. Bellusci contributed equally to this article as lead authors and supervised the work.

Corresponding author: Saverio Bellusci (saverio.bellusci@innere.med.uni-giessen.de)

Shareable abstract (@ERSpublications)
A novel population of AT2 progenitor cells enriched for PD-L1 has been identified. This normally quiescent subpopulation of AT2 cells becomes highly proliferative and differentiates into mature AT2 in response to alveolar injury. https://bit.ly/31G0IIW

Cite this article as: Ahmadvand N, Khosravi F, Lingampally A, et al. Identification of a novel subset of alveolar type 2 cells enriched in PD-L1 and expanded following pneumonectomy. Eur Respir J 2021; 58: 2004168 [DOI: 10.1183/13993003.04168-2020].

Abstract

Alveolar type 2 (AT2) cells are heterogeneous cells, with specialised AT2 subpopulations within this lineage exhibiting stem cell properties. However, the existence of quiescent, immature cells within the AT2 lineage that are activated during lung regeneration is unknown.

Sftpc^CreERT2/+;tdTomato^flox/flox mice were used for the labelling of AT2 cells and labelled subpopulations were analysed by flow cytometry, quantitative PCR, assay for transposase-accessible chromatin using sequencing (ATAC-seq), gene arrays, pneumonectomy and culture of precision-cut lung slices. Single-cell RNA-sequencing (scRNA-seq) data from human lungs were analysed.

In mice, we detected two distinct AT2 subpopulations, with low tdTomato level (Tom^Low) and high tdTomato level (Tom^High). Tom^Low cells express lower levels of the AT2 differentiation markers *Fgfr2b* and *Etv5*, while Tom^High, as *bona fide* mature AT2 cells, show higher levels of *Sftpc*, *Sftpb*, *Sftpa1*, *Fgfr2b* and *Etv5* expression. ATAC-seq analysis indicates that Tom^Low and Tom^High cells constitute two distinct cell populations, with specific silencing of *Sftpc*, *Rosa26* and cell cycle gene loci in the Tom^Low population. Upon pneumonectomy, the number of Tom^Low but not Tom^High cells increases and Tom^Low cells show upregulated expression of *Fgfr2b*, *Etv5*, *Sftpc*, *Ccnd1* and *Ccnd2* compared to Sham. Tom^Low cells overexpress programmed cell death 1 ligand 1 (PD-L1), an immune inhibitory membrane receptor ligand, which is used by flow cytometry to differentially isolate these two subpopulations. In the human lung, data mining of a recent scRNA-seq AT2 data set demonstrates the existence of a *PD-L1^Pos* population. Therefore, we have identified a novel population of AT2 quiescent, immature progenitor cells in mouse that expand upon pneumonectomy and we have provided evidence for the existence of such cells in human.

Introduction

Alveolar type 2 (AT2) progenitor cells display self-renewal capabilities to maintain the AT2 cell pool and differentiate into AT1 cells following lung injury [1–5]. However, it is still debatable whether quiescent

and immature AT2 progenitor cells exist in mouse and human lungs and if surface markers can be used to isolate these cells.

In rodents, AT2 cells are heterogeneous. Different subpopulations within this lineage, with different stem cell properties, have been identified based on various markers such as E-cadherin (E-CAD), AXIN2, integrin α6β4 and the dual expression of surfactant protein C (SFTPC)/secretoglobin family 1A member 1 (SCGB1A1) [6–9]. AT2 cells can be divided equally into E-CAD^{Pos} and E-CAD^{Neg} cells. E-CAD^{Neg} cells are more resistant to hyperoxia injury, more proliferative and display higher level of telomerase activity, while E-CAD^{Pos} cells are more sensitive to damage [6]. In the adult mouse lung, AXIN2^{Pos} cells make up 1% of the mature AT2 (SFTPC^{High}) cells and are distributed throughout the lung [8]. This ratio of AXIN2^{Pos} cells is stable over time. *In vivo* lineage tracing of AXIN2^{Pos} (SFTPC^{High}) cells revealed their ability to form clones of two to five cells accompanied by their expansion and differentiation into AT1 expressing podoplanin (PDPN). In addition, these cells display enhanced self-renewal capabilities in alveolosphere assays compared to the AXIN2^{Neg} AT2 cells, suggesting that these AXIN2^{Pos} cells represent a subpopulation of mature AT2 cells with enhanced stem cell capacities [8]. In a similar and independent study, AXIN2^{Pos} cells belonging to the mature AT2 cell population were characterised. These cells, called alveolar epithelial progenitor (AEP) cells, comprise ~20% of adult mature AT2 cells and are enriched for WNT target genes and developmental genes such as *Fgfr2*, *Nkx2.1*, *Id2*, *Etv4*, *Etv5* and *Foxa1*. These cells also display increased self-renewal ability in alveolospheres compared to total AT2 cells [9].

AT2 cell heterogeneity is not limited to the adult lung. During the alveologenesis phase of lung development, AXIN2^{Pos} AT2 cells display enhanced proliferation compared to total AT2 cells [10]. A subset of SFTPC^{Neg}, laminin receptor integrin α6β4^{Pos} cells, located at the bronchoalveolar duct junctions (BADJ) and within the alveoli, regenerate AT2 SFTPC^{Pos} cells in the alveoli after severe lung injury [7]. Finally, bronchoalveolar stem cells, positive for the alveolar marker SFTPC and the club cell marker SCGB1A1, are located at the BADJ and are amplified upon injury to give rise to either alveolar epithelial cells or club cells [11–13]. AT2 cell heterogeneity was equally shown in the context of diphtheria toxin injury, with a subpopulation of lineage-labelled AT2 cells displaying relatively more resistance to diphtheria toxin toxicity able to repopulate the AT2 pool following injury. The identity of these survivor cells, however, is not clear [3].

In the present study, we identified a novel population of AT2 quiescent and immature progenitor cells characterised by low *Sftpc* level and high expression of the surface marker programmed cell death 1 ligand 1(PD-L1) (also known as CD274), an immune checkpoint protein expressed in cancer stem cells and mediating anti-tumour suppression response [14–16]. We deployed a series of *in vivo* approaches in mice to label different subpopulations of AT2 cells, examined their epigenetic and transcriptomic characteristics, and tested their respective response *in vivo* during lung regeneration following pneumonectomy as well as *in vitro* using the culture of precision-cut lung slices (PCLS). We also validated the use of PD-L1 antibodies to differentially sort epithelial subpopulations and carried out data mining of recently published AT2 single-cell RNA-sequencing (scRNA-seq) experiments. Our work opens the way for an in-depth characterisation of this novel quiescent and immature AT2 stem cell population.

Materials and methods

Animal experiments
All animal studies were performed according to protocols approved by the Animal Ethics Committee of the Regierungspraesidium Giessen (permit numbers: G7/2017–No.844-GP and G11/2019–No. 931-GP).

Pneumonectomy
See supplementary material.

Lung dissociation and fluorescence-activated cell sorting
Single-cell suspension was generated from adult lungs and stained with anti-EPCAM (APC-Cy7-conjugated, Biolegend, 1:50), CD49F (APC-conjugated, Biolegend, 1:50), anti-PDPN (FITC-conjugated, Biolegend, 1:20) and anti-PD-L1 (unconjugated, Thermo Fisher, 1:100) antibodies for 20 min on ice in the dark, followed by washing. The cells were then stained for goat anti-rabbit secondary antibody Alexa fluor 488 (Invitrogen, 1:500) for 20 min on ice in the dark. Next, cells were washed and stained with SYTOX (Invitrogen), a live/dead cell stain, according to the manufacturer's instructions. Flow cytometry data acquisition and cell sorting were carried out using a FACSAria III cell sorter (BD Biosciences). Data were analysed using FlowJo software version X (FlowJo, LLC).

See supplementary material for the mouse lung dissociation.

RNA extraction and quantitative real-time PCR
See supplementary material.

Immunofluorescence staining
See supplementary material.

Alveolosphere assay
See supplementary material.

Microarray
See supplementary material.

ATAC-seq
See supplementary material.

Mining of scRNA-seq data set for human AT2 cells
For the analysis, we used the synapse ID (syn21041850) data set deposited at https://www.synapse.org/#!Synapse:syn21041850/wiki/600865 and published by TRAVAGLINI *et al.* [17]. The Seurat objects were updated to Seurat v3 [18] and AT2 cells were extracted using the subset' function. The data set was reanalysed starting from raw counts using the SCTransform wrapper in Seurat. Data imputation was then performed using a low-rank approximation with the package ALRA [19].

Quantification and statistical analysis
For quantification of immunofluorescence, cells were counted in 10 independent 63× fields per sample. Statistical analysis and graph assembly were carried out using GraphPad Prism 6 (GraphPad Prism Software). Significance was determined by unpaired two-tailed t-tests. Data are presented as mean±SEM. Values of $p < 0.05$ were considered significant. The number of biological samples (n) for each group is stated in the corresponding figure legends.

Results

Identification of two AT2 subpopulations with different Sftpc and Fgfr2b levels

$Sftpc^{CreERT2/+};tdTomato^{flox/flox}$ mice were used to lineage label AT2 cells in the adult lung. In our experimental approach, tamoxifen was delivered in the water for 1 week. Two distinct subpopulations of tdTomato^{Pos} (Tom^{Pos}) cells, that we called tdTomato^{Low} (Tom^{Low}) and tdTomato^{High} (Tom^{High}), were identified using flow cytometry analysis (figure 1a–c). Of note, a similar observation, which was not followed up, was previously reported using the $Sftpc^{Cre-ER}$ mouse line generated by FINN *et al.* [20]. On average, Tom^{Low} cells represented 9.93±1.73% of the overall EPCAM^{Pos} cells (n=4) and Tom^{High} cells represented 42.75±1.22% of the overall EPCAM^{Pos} cells (n=4). Out of the total Tom^{Pos} cells, on average 17.58±2.52% (n=4) were Tom^{Low} and 81.93±2.3% (n=4) were Tom^{High}. We also determined the extent of recombination of the *LoxP-STOP-LoxP-tdTomato* cassette in the isolated Tom^{Low} and Tom^{High} cells. Our results indicate that complete recombination was observed in Tom^{High} while incomplete recombination was observed in Tom^{Low}, indicated by the presence of the 795 bp stop codon band (figure 1d). This result suggested either contamination of the Tom^{Low} pool by non-AT2 cells or the lack of access of Cre to the *LoxP-STOP-LoxP-tdTomato* cassette in the *Rosa26* locus of Tom^{Low} cells. The presence of the two subpopulations based on Tomato intensity could also be explained by improper recombination of either one or two copies of the LoxP-STOP-LoxP-tdTomato cassette in $tdTomato^{flox/flox}$ mice. To test these different possibilities, we carried out a similar experiment with $Sftpc^{CreERT2/+};tdTomato^{flox/+}$ mice, which exhibit only one copy of the *LoxP-STOP-LoxP-tdTomato* cassette (figure 1e–h). Similarly, we found two subpopulations of Tom^{Pos} cells and, importantly, complete recombination of the *LoxP-STOP-LoxP-tdTomato* cassette in Tom^{Low}, indicating the absence of contamination by non-AT2 cells in the Tom^{Low} pool. This conclusion is supported by our quantitative PCR (qPCR) data for markers of endothelial, hematopoietic, macrophage and fibroblast cells (supplementary figure S1). Overall, our data support the existence of two AT2 cell subpopulations in $Sftpc^{CreERT2/+};tdTomato^{flox/flox}$ lungs, based on different levels of *Tomato* expression. This is due to the differential expression of *Tomato per se* from the *Rosa26* promoter in Tom^{High} *versus* Tom^{Low} cells. In addition, in $Sftpc^{CreERT2/+};tdTomato^{flox/flox}$ lungs, this is also associated with the incomplete recombination of the *LoxP-STOP-LoxP* cassette, which is also located in the *Rosa26* locus.

We also confirmed that epithelial cells were specifically labelled in this mouse line and the labeling mostly targeted AT2 SFTPC^{Pos} cells (supplementary figure S2). Very few BACS cells, identified through their localisation at the BADJ, were labelled (0.1% of the total Tom^{Pos} cells, data not shown), consistent with the literature [7]. Our labelling efficiency of AT2 cells was 77±5.40% (n=4) (supplementary figure S2b).
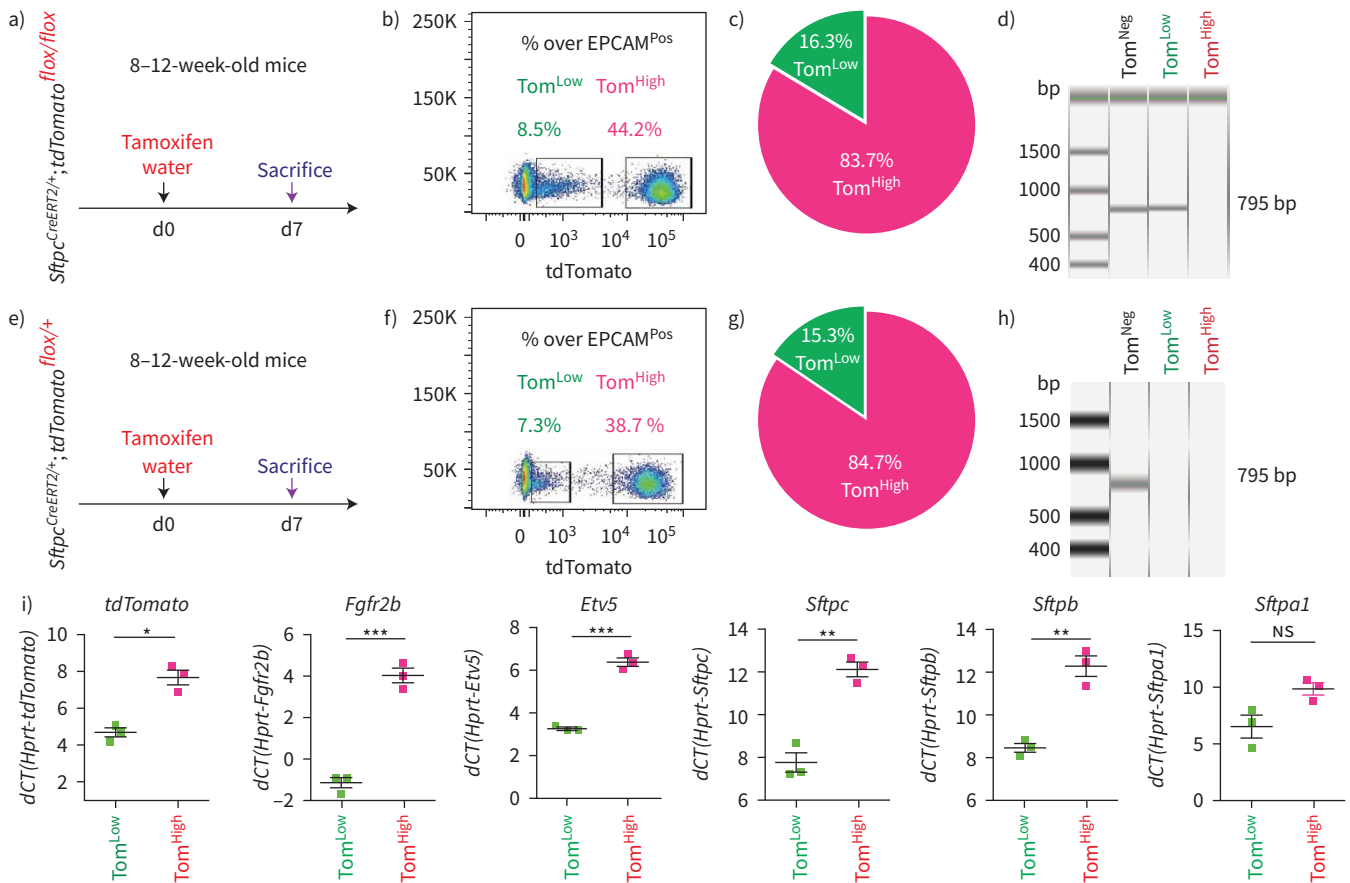
FIGURE 1 Identification of two subpopulations of AT2-lineage-labelled cells, named tdTomato^Low (Tom^Low) and tdTomato^High (Tom^High). a) Timeline of tamoxifen treatment of *Sftpc^{CreERT2/+};tdTomato^{flox/flox}* mice (n=4). d: day. b) Representative flow cytometry of EPCAM^Pos population selection and identification of Tom^Low (8.5%) and Tom^High (44.2%) populations based on the tdTomato level. c) Percentage of Tom^Low (16.3%) and Tom^High (83.7%) in total tdTomato^Pos cells. d) PCR on genomic DNA isolated from fluorescence-activated cell sorting (FACS)-based sorted Tom^Low and Tom^High cells from *Sftpc^{CreERT2/+};tdTomato^{flox/flox}* mice for Stop codon. e) Timeline of tamoxifen treatment of *Sftpc^{CreERT2/+};tdTomato^{flox/+}* mice and f) representative flow cytometry analysis of Tom^Low (7.3%) and Tom^High (38.7%). g) The pie chart shows the percentage of Tom^Low (15.3%) and Tom^High (84.7%) in total tdTomato^Pos cells. h) PCR on genomic DNA isolated from FACS-based sorted Tom^Low and Tom^High cells from *Sftpc^{CreERT2/+};tdTomato^{flox/+}* mice. i) Quantitative PCR analysis of FACS-based sorted Tom^Low and Tom^High cells for the expression of *Tomato*, *Fgfr2b*, *Etv5*, *Sftpc*, *Sftpb* and *Sftpa1*. dCT: delta cycle threshold. Data are presented as mean±SEM. *: p<0.05; **: p<0.01; ***: p<0.001.

In this mouse line, 4.5% of Tom^Pos/total cells were labelled in mice exposed to normal water, indicating leakiness. This percentage increased to 20.5% of Tom^Pos/total cells in mice exposed to tamoxifen water for 1 week (supplementary figure S3), indicating robust induction of labelling. We also carried out labelling at 8 weeks of age by exposing the mice to tamoxifen water for 1 week followed by a 6- and 9-months chaseperiod. Our data indicate that both Tom^Low and Tom^High subpopulations were detected at these two time points, and were stable populations (supplementary figure S4).

Next, qPCR was performed on fluorescence-activated cell sorting (FACS)-isolated Tom^Low and Tom^High cells. Our results show that *Fgfr2b* and its associated downstream target *Etv5*, as well as the differentiation markers *Sftpc*, *Sftpb* and *Sftpa1*, were significantly enriched in Tom^High *versus* Tom^Low cells (figure 1i). Thus, we conclude that Tom^High represents the *bona fide* mature AT2 cells and we hypothesised that the lineage-related Tom^Low cells represent immature AT2 cells.

ATAC-seq analysis indicates that Tom^Low cells and Tom^High cells are distinct cell populations

To carry out genome-wide profiling of the epigenomic landscape, an assay for transposase-accessible chromatin using sequencing (ATAC-seq) was performed on Tom^Low and Tom^High subpopulations (figure 2a). Common and distinct peaks were identified for Tom^Low and Tom^High cells (figure 2b–d).
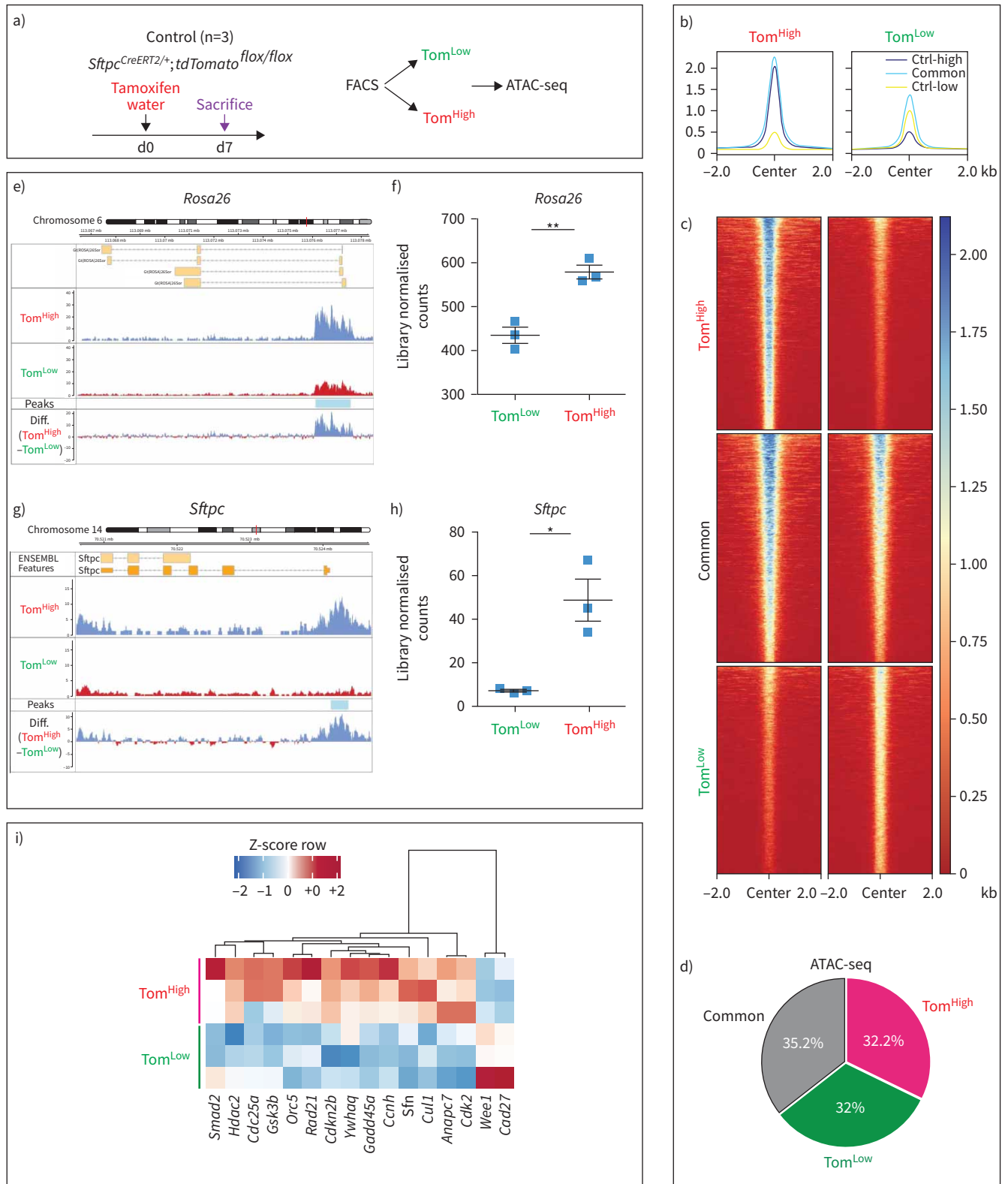
FIGURE 2 Assay for transposase-accessible chromatin using sequencing (ATAC-seq) analysis on fluorescence-activated cell sorting (FACS)-based sorted tdTomato^{Low} (Tom^{Low}) and tdTomato^{High} (Tom^{High}) populations. a) Timeline of tamoxifen treatment of $Sftpc^{CreERT2/+};tdTomato^{flox/flox}$ mice (n=3). ATAC-seq was carried out on FACS-based sorted Tom^{Low} and Tom^{High} subpopulations. d: day. b, c) Coverage heat maps of Tom^{Low} and Tom^{High}, displaying genome-wide regions of differential open chromatin peaks in Tom^{Low} versus Tom^{High}. Tom^{Low} chromatin is less open and transcriptionally less active compared to Tom^{High}. Ctrl-low shows the peaks related to open chromatin regions in Tom^{Low}. Ctrl-high shows the peaks related to open chromatin regions in Tom^{High}. Common shows peaks detected in both Tom^{Low} and Tom^{High} subpopulations. d) ATAC-seq

analysis of peaks based on the cut-offs shows 3605 upregulated in Tom^{High} (false discovery rate (FDR)<0.05, log$_2$(FC)>0.585, base mean>20), 3512 upregulated in Tom^{Low} (FDR<0.05, log$_2$(FC)>0.585, base mean>20) and 3878 non-regulated (base mean>20, FDR>0.5, log$_2$(FC) between −0.15 and 0.15), which means 32% and 32.2% of the genome is differently accessible in Tom^{Low} and Tom^{High}, respectively. e) ATAC-seq histogram of average read coverage at the *Rosa26* locus shows distinct ATAC-seq peaks at the promoter and denser chromatin in Tom^{Low} compared to Tom^{High} in this locus. Representative peaks of Tom^{Low} and Tom^{High} are the average of three independent samples. f) Quantification of peaks at the *Rosa26* locus. g) ATAC-seq profile at *Sftpc* locus shows distinct ATAC-seq peaks at the promoter and denser chromatin in Tom^{Low} compared to Tom^{High}. Representative peaks of Tom^{Low} and Tom^{High} are averages of three independent samples. h) Quantification of peak regions of *Sftpc* locus. The ATAC-seq data have been normalised for sequencing depth and the scale on the y-axis was chosen for optimal visualisation of peaks. i) ATAC-Heat-pVAI Z-score, Pearson, average heat map based on the ATAC-seq data of top cell cycle-related genes differentially regulated in Tom^{Low} and Tom^{High}. FDR: the significance of results by Benjamini–Hochberg correction of multiple tests (n=3).

Further analysis of the ATAC-seq data using the Reactome database indicated that the chromatin in loci of genes relating to metabolism, cholesterol metabolism, surfactant metabolism and triglyceride biosynthesis was more open in Tom^{High} cells. These data are in agreement with the known role of mature AT2 cells in surfactant production. By contrast, Tom^{Low} cells exhibit more accessibility for genes relating to the adaptive and innate immune system as well as genes involved in extracellular matrix (ECM) organisation, ECM proteoglycans and degradation of the ECM. These results suggest a new and important function for the Tom^{Low} cells in interactions with the immune system, potentially also displaying migratory capabilities through ECM degradation (supplementary figure S5a).

Our ATAC-seq data also support the observed decrease in *Tomato* (expressed from the *Rosa26* promoter) and *Sftpc* expression at the mRNA level in Tom^{Low} *versus* Tom^{High}. In the *Rosa26* and *Sftpc* loci, the peaks corresponding to the open chromatin configuration were detected at much higher levels in Tom^{High} than in Tom^{Low}, and this difference was confirmed to be statistically significant upon quantification (figure 2e–h). Interestingly, the analysis of ATAC-seq data also suggested that Tom^{Low} cells have reduced expression of cell cycle genes compared to Tom^{High} cells (figure 2i). This decrease in cell cycle genes was confirmed by the analysis of our gene array data between Tom^{Low} and Tom^{High} (supplementary figure S5b). Overall our data indicate that in homeostatic conditions the Tom^{Low} cells fit the profile of a quiescent population.

AT2 Tom^{Low} and Tom^{High} display different colony-forming capabilities

To compare the self-renewal capacity of Tom^{Low} and Tom^{High}, FACS-based sorted cells were co-cultured with CD31^{Neg}CD45^{Neg}EPCAM^{Neg}SCA1^{Pos} resident lung mesenchymal cells according to a previously published protocol (figure 3a). Tom^{High} behaved as *bona fide* AT2 cells, forming alveolospheres with the expected colony-forming efficiency (figure 3b, d, e) [3, 9, 21], whereas Tom^{Low} displayed very weak organoid-forming capabilities, which is in line with their proposed quiescent status. Both populations transdifferentiated into receptor for advanced glycation end-products (RAGE)-positive AT1 cells after 14 days in culture (figure 3c).

Expansion of Tom^{Low} population following pneumonectomy

A critical question regarding these two subpopulations of AT2 cells is whether they are differentially engaged in the context of lung regeneration. Therefore, we used the mouse pneumonectomy (PNX) model to trigger lung regeneration, a process that is tightly associated with the proliferation of AT2 cells [22, 23]. *Sftpc*$^{CreERT2/+}$;*tdTomato*$^{flox/flox}$ mice (n=4) were treated with tamoxifen water for 1 week to label the AT2 lineage. The mice were then put on normal water for 2 weeks to ensure enough time for tamoxifen clearance. Unilateral left lung pneumonectomy was then performed to induce the process of compensatory growth in the remaining right lobes. Control mice (Sham) underwent the same process but without removing the left lobe (figure 4a). The animals were killed on day 7 post-surgery and the right lobes were processed for FACS. Because the accessory lobe has been shown to respond the most to PNX [24], our results are likely underestimating the response of Tom^{Low} cells in the context of PNX. The quantification of the abundance of Tom^{Low} and Tom^{High} cells over the total number of EPCAM^{Pos} cells in Sham and PNX mice indicates that the ratio of Tom^{High} cells/total number of EPCAM^{Pos} cells remained unchanged between two conditions, while the ratio of Tom^{Low} cells was significantly increased in the context of PNX *versus* Sham (figure 4b–d). This suggests that it is the Tom^{Low} cells, rather than the previously thought Tom^{High} cells, that are contributing to the process of lung regeneration. These two AT2 populations were isolated by FACS for further analysis by qPCR. Upon PNX, the expression of *Fgfr2b*, *Etv5*, *Sftpc*, *Cyclin D1* (*Ccnd1*) and *Cyclin D2* (*Ccnd2*) was significantly upregulated in Tom^{Low}. A trend towards an increase was also observed in *Ki67* expression (figure 4e). These results are consistent with FGFR2b signalling activation and proliferation in Tom^{Low} cells in the context of lung regeneration. By contrast, Tom^{High} cells showed no difference in *Fgfr2b*, *Etv5* or *Sftpc* between PNX and Sham conditions (figure 4f). Surprisingly, we noticed an increase in *Ki67*, *Ccnd1* and *Ccnd2* (figure 4f) but because the number of
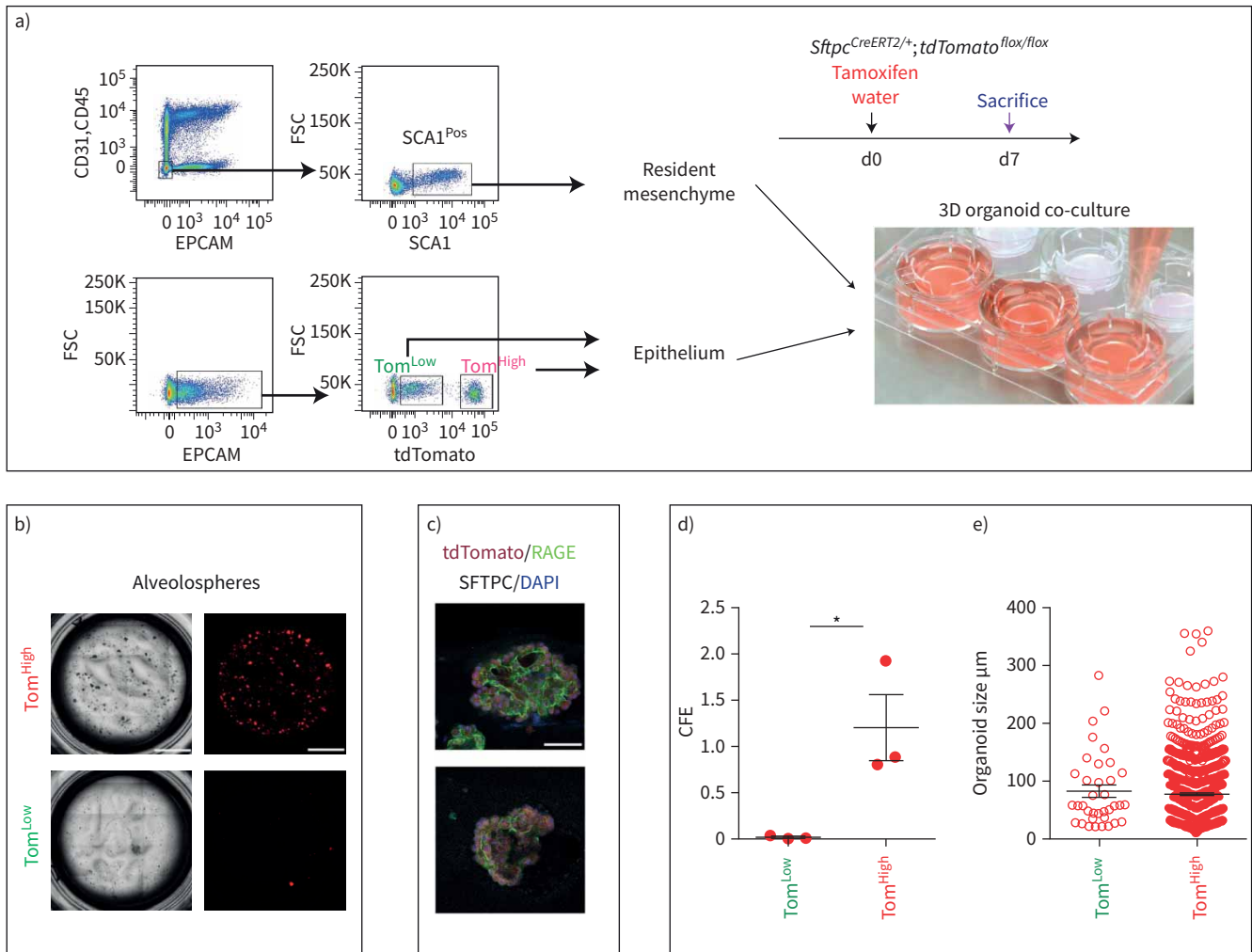
FIGURE 3 Different colony-forming capabilities of tdTomato^{Low} (Tom^{Low}) and tdTomato^{High} (Tom^{High}) cells. a) Representative flow cytometry shows the gating strategy of CD31^{Neg} CD45^{Neg} EPCAM^{Neg} population and further selection of SCA1^{Pos} resident mesenchymal cells from C57BL/6 lungs (upper plot), as well as the selection of Tom^{Low} and Tom^{High} from the EPCAM^{Pos} population from *Sftpc$^{CreERT2/+}$;tdTomato$^{flox/flox}$*(lower plot). Mesenchymal cells were co-cultured with Tom^{Low} and Tom^{High} separately (n=3). d: day. b) Representative alveolospheres from Tom^{Low} and Tom^{High} (n=3). Scale bar: 100 μm. c) Representative SFTPC and RAGE immunofluorescence staining of alveolospheres after 14 days in culture. Scale bar: 50 μm. d) Quantification of colony-forming efficiency (CFE) and e) alveolospheres size in Tom^{High} and Tom^{Low} (n=3). Data are presented as mean±SEM. *: p<0.05.

Tom^{High} cells was not increased in PNX *versus* Sham mice, the significance of these results is not clear. We also carried out the labelling of proliferative cells using a single dose of intraperitoneal 5-ethynyl-2-deoxyuridine (EdU) (0.1 mg·g^{-1} of mouse) at day 6 following PNX. We analysed the lungs at day 7 (1-day chase period, n=2 mice) and day 14 (8-day chase period, n=3 mice). AT2 PD-L1^{Pos} (equivalent to the Tom^{Low}) and AT2 PD-L1^{Neg} (equivalent to the Tom^{High}) were isolated by FACS. We performed cytospins with these isolated cells and carried out immunofluorescence for EdU. While it was easy to observe numerous AT2 PD-L1^{Neg} cells, the number of AT2 PD-L1^{Pos} cells on the slides was very low, making it difficult to analyse EdU incorporation in these cells. Our results indicated that 2.3±0.8% (n=2 independent mice, 300 cells counted per mice) of the AT2 PD-L1^{Neg} were EdU^{Pos} at day 7. However, at day 14, 12.2±0.4% were EdU^{Pos} (n=3 mice, 300 cells per mouse). The increase in the number of labelled cells between these two time points, after an 8-day chase period, suggests that the EdU^{Pos} cells in the AT2 PD-L1^{Neg} pool are coming from the AT2 PD-L1^{Pos} cells (data not shown).

Loss of Tom^{High} cells leads to expansion of Tom^{Low} cells
We made use of PCLS to follow the fate of Tom^{Pos} cells over time *in vitro*. Our flow cytometry results indicate that this approach leads to the drastic loss of Tom^{High} cells (figure 5a, b). Therefore, we took
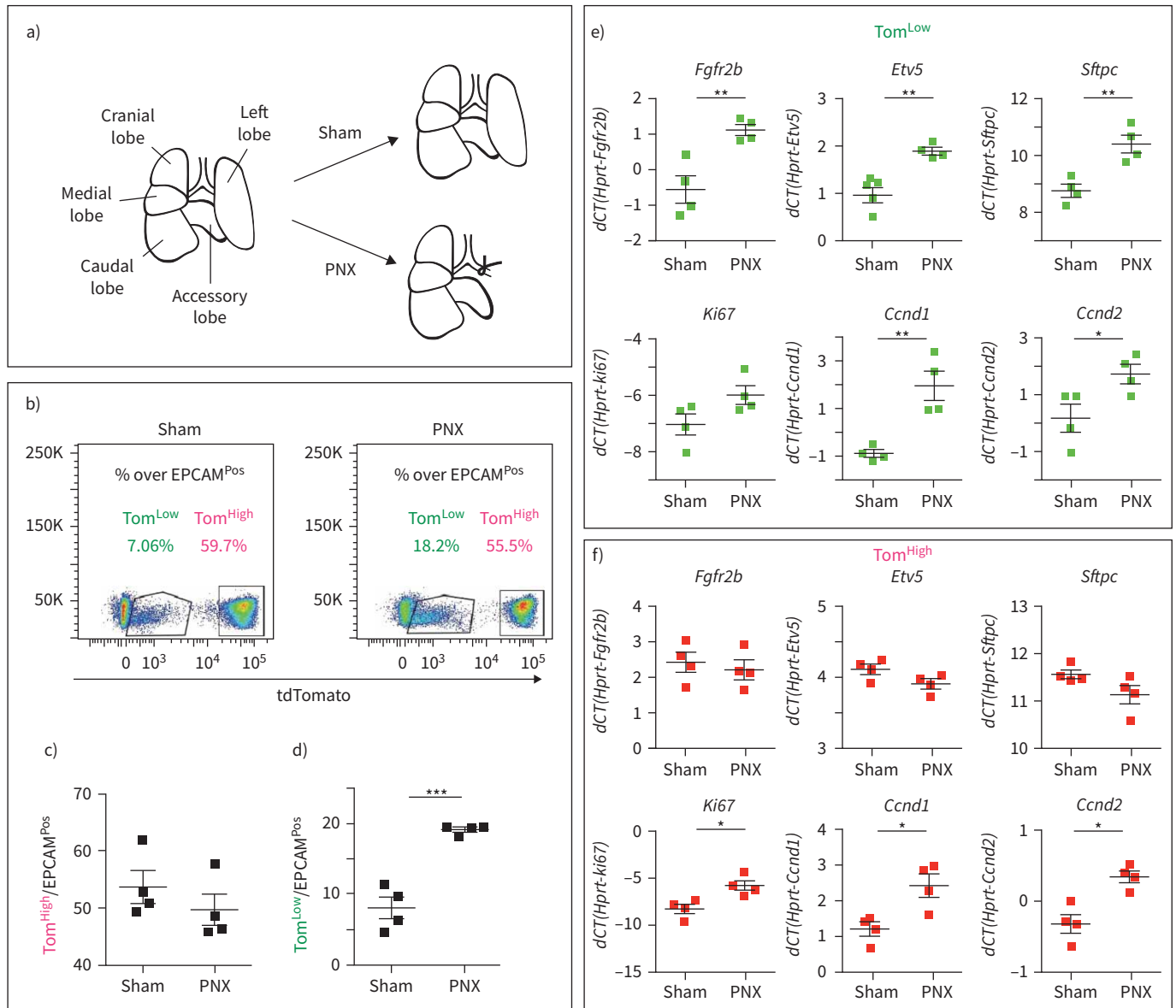
FIGURE 4 Expansion of tdTomato^{Low} (Tom^{Low}) but not tdTomato^{High} (Tom^{High}) following pneumonectomy (PNX). a) Schematic representation of the PNX and Sham models. b) Representative flow cytometry analysis of Tom^{Low} and Tom^{High} populations 7 days after PNX and Sham, and quantification of c) Tom^{High} and e) Tom^{Low} percentages in EPCAM^{Pos} population between Sham and PNX groups (n=4). f) Quantitative PCR (qPCR) analysis of fluorescence-activated cell sorting (FACS)-based sorted Tom^{Low} population for expression of *Fgfr2b*, *Etv5*, *Sftpc*, *Ki67*, *Ccnd1* and *Ccnd2*. g) qPCR analysis of FACS-based sorted Tom^{High} population for expression of *Fgfr2b*, *Etv5*, *Sftpc*, *Ki67*, *Ccnd1* and *Ccnd2*. Data are presented as mean±SEM. dCT: delta cycle threshold. *: $p<0.05$; **: $p<0.01$; ***: $p<0.001$.

advantage of this system to monitor the fate of Tom^{Low} cells over time after a massive loss of Tom^{High}. Over a culture period of 96 h, we observed the formation of cell clusters and a significant increase in tdTomato intensity (figure 5c), suggesting the differentiation of Tom^{Low} cells towards mature (Tom^{High}) AT2 cells. In addition, we observed the presence of clusters of Tom^{Pos} cells at 240 h (figure 5c). We also performed video-fluorescence microscopy to track individual Tom^{Low} cells (n=6) in PCLS over a period of 45 h. Our results indicated that the intensity of the tdTomato signal in these cells progressively increased with time, thereby confirming the transition from Tom^{Low} to Tom^{High} status (data not shown). Finally, we analysed apoptosis and proliferation in these PCLS over time. Our results indicated a very significant increase in tdTomato^{Pos}TUNEL^{Pos} over total tdTomato^{Pos} cells (figure 5d–k) in PCLS at 20 h, which is in line with the lack of detection of Tom^{High} cells by FACS at that time point (figure 5b). In addition, proliferation analysis indicated a robust increase in the number of tdTomato^{Pos}EdU^{Pos} over total
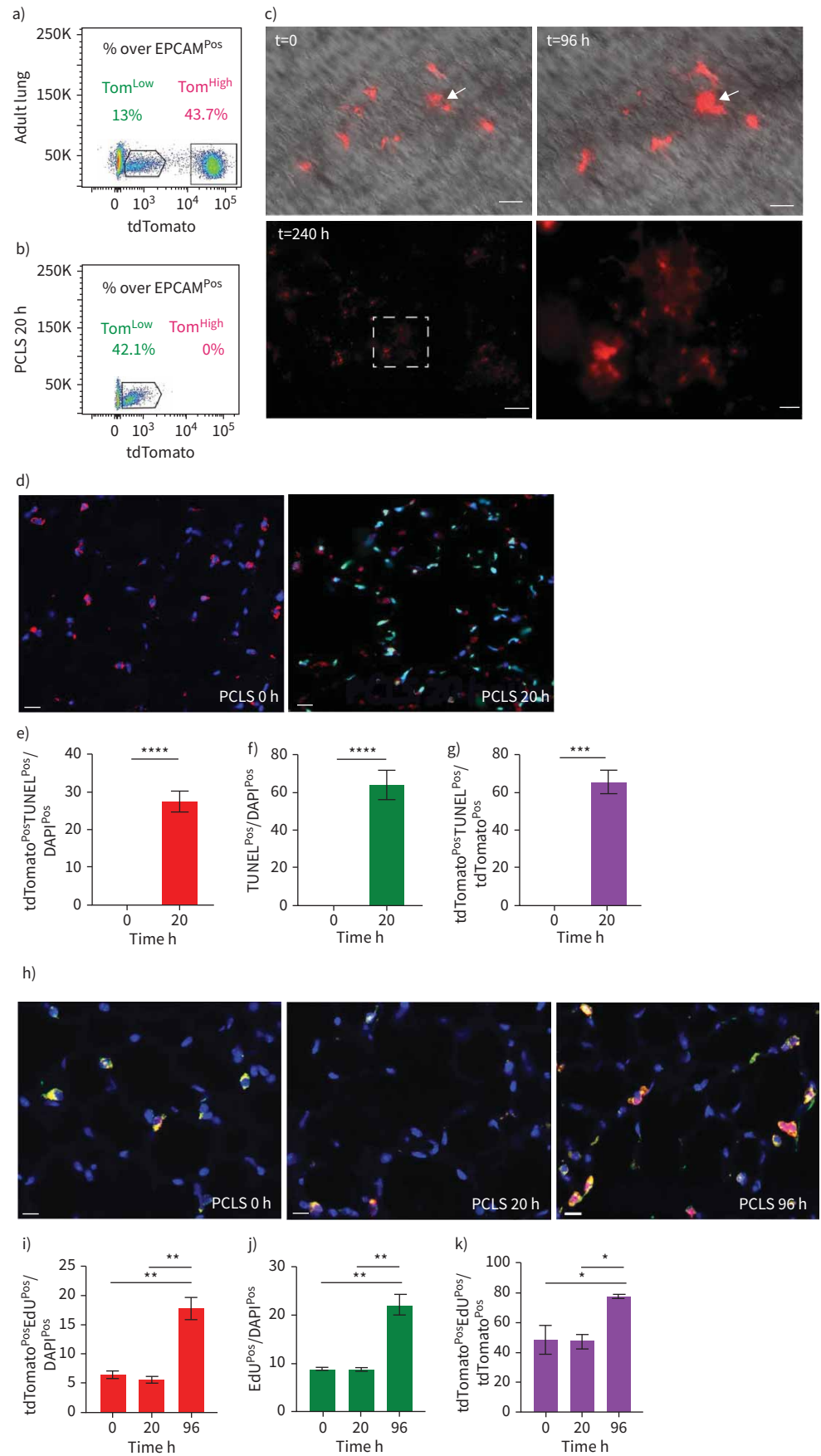
FIGURE 5 Characterisation of the fate of tdTomato^{Low} (Tom^{Low}) cells in precision-cut lung slices (PCLS). a, b) Representative flow cytometry analysis of Tom^{Low} and tdTomato^{High} (Tom^{High}) before processing the lungs for PCLS in freshly generated PCLS (a) and PCLS after 20 h culture (b). c) Visualisation of the Tom^{Low} in PCLS at t=0, t=96 h and t=240 h. Arrows indicate the formation of cell clusters. Scale bars: 250 µm (low magnification) and 50 µm (high magnification). d) Analysis of apoptosis with representative terminal deoxynucleotidyl transferase dUTP nick end labelling (TUNEL) immunofluorescence staining on the PCLS (scale bar: 50 µm) and quantification of e) tdTomato^{Pos} TUNEL^{Pos} cells out of total cells, f) TUNEL^{Pos} cells out of total cells and g) tdTomato^{Pos} TUNEL^{Pos} cells out of tdTomato^{Pos} cells (n=4). Data are presented as mean±SEM. h) Analysis of proliferation with representative EdU immunofluorescence staining on the PCLS (scale bar: 50 µm) and quantification of i) tdTomato^{Pos} EdU^{Pos} cells out of total cells, j) EdU^{Pos} cells out of total cells and k) tdTomato^{Pos} EdU^{Pos} cells out of tdTomato^{Pos} cells (n=4). Data are presented as mean±SEM. *: p<0.05; **: p<0.01; ***: p<0.001; ****: p<0.0001.

tdTomato^{Pos} cells in PCLS between 20 h and 96 h (figure 5h–k), supporting our previous conclusion in the context of PNX that the Tom^{Low} cells are proliferating after injury.

PD-L1 is a specific surface marker enriched in Tom^{Low}

To identify markers differentially expressed between Tom^{Low} and Tom^{High}, we performed a gene array on FACS-isolated Tom^{Low} and Tom^{High} cells (figure 6a, supplementary figure S5b). Among the 100 top genes differentially expressed in Tom^{Low} *versus* Tom^{High} cells, three cell surface markers, *Cd33*, *Cd300lf* and *Cd274* (also known as *Pd-l1*), were identified as being enriched in Tom^{Low} compared to Tom^{High}. qPCR analysis confirmed the significantly higher expression of *Cd33* and *Pd-l1* in Tom^{Low} compared to Tom^{High} (figure 6b). PD-L1 is an interesting marker because it is an immune inhibitory receptor ligand and its expression is highly increased in adenocarcinoma [14, 25]. The use of this marker is also relevant because our ATAC-seq analysis revealed that Tom^{Low} cells are enriched in genes belonging to the immune system (supplementary figure S5a). The use of PD-L1 as a surface marker enriched in Tom^{Low} cells was further validated using PD-L1 immunofluorescence staining and flow cytometry. To this end, PD-L1 immunofluorescence staining on cytospins confirmed a higher level of protein at the plasma membrane in Tom^{Low} than in Tom^{High} cells (figure 6c). Moreover, flow cytometry analysis of Tom^{Low} and Tom^{High} populations separately showed that 46.9% of Tom^{Low} cells were PD-L1^{Pos} while only 0.77% of Tom^{High} cells were PD-L1^{Pos} (figure 6d). In addition, PD-L1 immunofluorescence staining on lung sections localise tdTomato^{Pos} PD-L1^{Pos} cells in the alveoli (figure 6e). In conclusion, these results suggest that PD-L1 antibodies could be instrumental in differentially isolating the equivalent of Tom^{Low} *versus* Tom^{High} in wild-type lungs.

Identification of AT2 PD-L1^{Pos} SFTPC^{Low} in the lungs of wild-type mice

To address whether PD-L1 could be used to isolate the equivalent of Tom^{Low} and Tom^{High} without the need for a lineage tracing approach, FACS-based analysis was performed on isolated C57BL/6 lungs. The PD-L1 antibody was initially validated to show its expression in alveolar macrophages by immunofluorescence staining (in a lower magnification image of figure 6e) and flow cytometry (supplementary figure S6c). AT2 cell selection was based on the gating of EPCAM^{Pos}, CD49f^{Intermediate} (to label the alveolar epithelial cells), PDPN^{Neg} population (to exclude the AT1 cells), from which the percentages of PD-L1 positive and negative cells were analysed (figure 7a). On average, 8.99±0.51% (n=4) of these AT2 cells were PD-L1^{Pos} and 90.23±0.58% (n=4) were PD-L1^{Neg} (figure 7a). This ratio is consistent with the finding that most (80%) of the lineage-traced AT2 cells were composed of Tom^{High} (PD-L1^{Neg}) cells (figure 1c). qPCR analysis on sorted PD-L1^{Pos} and PD-L1^{Neg} AT2 cells indicated a higher level of *Fgfr2b*, *Etv5* and *Sftpc* in PD-L1^{Neg} than PD-L1^{Pos} cells (figure 7b–d). This result is also in line with PD-L1^{Neg} cells corresponding to Tom^{High} cells, while the expression profile of PD-L1^{High} fits with these cells being the equivalent of the Tom^{Low}. Finally, flow cytometry analysis of alveolar epithelial cells (EPCAM^{Pos}, CD49f^{inter}) stained with SFTPC and PD-L1 identified a subpopulation of AT2 cells (6.8%) displaying a low level of SFTPC and a high level of PD-L1 (figure 7e). This SFTPC^{Low} PD-L1^{High} cluster likely contains the Tom^{Low} cells.

qPCR analysis was carried out to validate the potential contamination of isolated AT2 PD-L1^{Pos} and AT2 PD-L1^{Neg} cells. Our results confirm the lack of contamination of these two subpopulations by endothelial, hematopoietic, macrophage and fibroblast cells (supplementary figure S6). In addition, co-culturing these cells with resident SCA1^{Pos} mesenchymal cells in alveolosphere assay indicated that only AT2 PD-L1^{Neg} cells (the equivalent of Tom^{High} cells) display self-renewal capabilities (supplementary figure S7). Finally, there were also higher numbers of AT2 PD-L1^{Pos} cells in PNX *versus* Sham (supplementary figure S8).
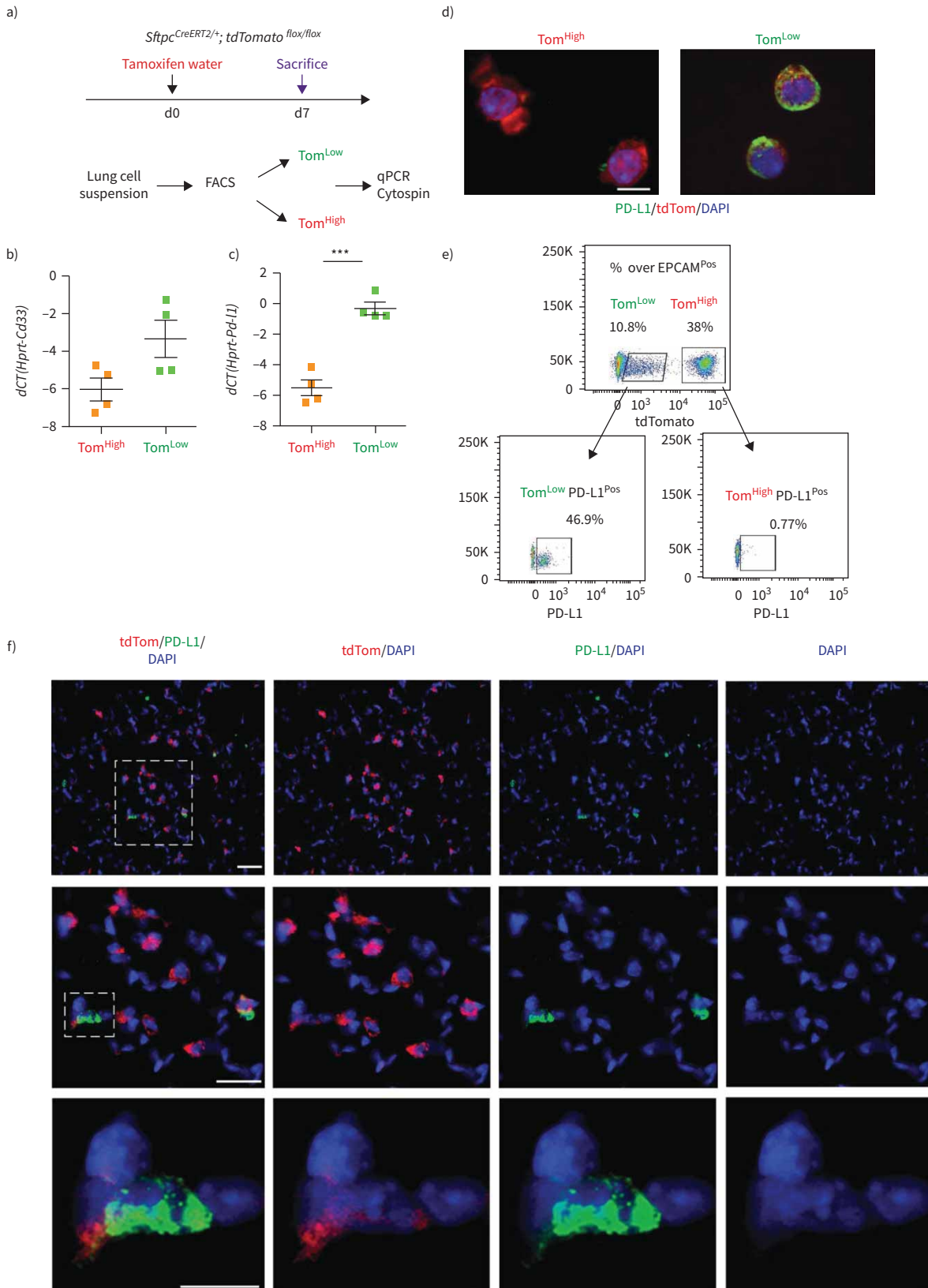
FIGURE 6 PD-L1 is a specific surface marker enriched in tdTomato^{Low} (Tom^{Low}) cells. a) Validation of gene array data by quantitative PCR (qPCR). d: day. b, c) Quantification of the expression levels of *Cd33* (b) and *Pd-l1* (c) in Tom^{Low} compared to tdTomato^{High} (Tom^{High}). Data are presented as mean±SEM. dCT: delta cycle threshold. ***: p<0.001. d) Representative PD-L1 immunofluorescence staining on Tom^{Low} and Tom^{High} cytospin cells. Scale bar: 50 μm.

e) Representative flow cytometry analysis of PD-L1^{Pos} population in Tom^{Low} and Tom^{High}. f) Representative PD-L1 immunofluorescence staining on the lung sections. Scale bar: 10 μm.

Altogether, our data indicate that the AT2 PD-L1^{Pos} and AT2 PD-L1^{Neg} cells are the functional equivalent of Tom^{Low} and Tom^{High}, respectively.

Identification of PD-L1^{Pos} cells in a human AT2 scRNA-seq data set

The scRNA-seq results from a recent study reporting the global analysis of human lung cells [17] were used to further examine the presence of *PD-L1*^{Pos} cells in the human AT2 pool. Bioinformatic analysis using Uniform Manifold Approximation and Projection (UMAP) plots was carried out to improve the initial AT2 cell pool clustering. Our results allowed the initial AT2 cluster composed of 3198 cells to be separated into five sub-clusters (figure 8a). Analysis of *PD-L1* expression distinguished two positive clusters, named AT2 *PD-L1*^{High} and AT2-proliferative, displaying high levels of *PD-L1* (figure 8b, green and lavender arrows, respectively). Note that the AT2-proliferative cluster had higher expression of *MIK67* and *PCNA* (supplementary figure S9). However, because the AT2-proliferative cluster comprised only three cells, its relevance to our Tom^{Low} population identified in mice is not clear. The other sub-cluster (AT2 *PD-L1*^{High}) comprised 186 cells (5.82% of the initial AT2 pool). An analysis of gene expression is represented using a violin plot (figure 8b–d). Compared to the AT2 sub-cluster (labelled in red), *PD-L1* expression in AT2 *PD-L1*^{High} (labelled in green) was clearly increased (figure 8b). In addition, *FGFR2b* expression was not changed while *SFTPC* was only slightly decreased. However, lower expression of *AXIN2*, *SFTPA1* and *ETV5* was observed (figure 8d). It is therefore likely that the AT2 *PD-L1*^{High} sub-cluster is the human equivalent of the AT2 Tom^{Low} that we identified in mice. Interestingly, compared to the AT2 sub-cluster, the AT2-proliferative sub-cluster also displayed lower levels of *ETV5*, *SFTPC* and *SFTPA1* but a higher level of *AXIN2*. The genes enriched in AT2 *PD-L1*^{High} were also analysed (supplementary figure S10). Transmembrane 4L6 family member 1 (*TM4SF1*), a gene encoding a membrane protein, was highly enriched in AT2 *PD-L1*^{High} cells (figure 8d). Interestingly, this marker was used previously to isolate AEP cells, which are proposed to express high level of AXIN2 in the human lung [9]. It is clear that this marker is also expressed in AT2 *AXIN2*^{Low} *PD-L1*^{High} human cells (as well as in Tom^{Low} *versus* Tom^{High} in mice, data not shown), illustrating that more work is needed to characterise human and corresponding mouse progenitor cells and to identify more markers. Finally, we used the online resource of the IPF Cell Atlas to add further evidence for the presence of AT2 *PD-L1*^{Pos} cells in human lungs (data not shown). *CD274*^{Pos} (*PD-L1*^{Pos}) cells were observed in all four human data sets analysed (Banovitch/Kropski, Kaminski/Rosas, Lafyatis and Misharin). The level of expression of *ETV5*, *FGFR2* and *SFTPC* in AT2 *PD-L1*^{Pos} cells in these data sets fits with either their quiescence (low expression level) or activation (high expression level) (data not shown).

Discussion

We have identified a subpopulation of AT2 progenitor cells that is distinct from already identified mature AT2 progenitor subpopulations. Tom^{Low} cells are quiescent and immature cells in the steady state and, unlike AT2 AXIN2^{Pos} cells, express low levels of AT2 differentiation markers. Moreover, Tom^{Low} cells express significantly lower levels of *Axin2* than Tom^{High} cells in homeostasis, and *Axin2* expression in Tom^{Low} cells showed no change after PNX compared to the Sham condition (supplementary figure S11a, b). ZACHARIAS *et al.* [9] showed that AEPs express higher level of genes related to lung and tube development than mature AT2s. However, based on our gene array data, these genes are expressed at lower levels in Tom^{Low} compared with Tom^{High} cells (data not shown). This indicates that AEP cells are part of the Tom^{High} population. The newly identified Tom^{Low} cells are also different from the integrin α6β4 population because these cells are negative for *Sftpc* and, therefore, the *Sftpc*^{CreERT2} driver line cannot lineage trace this population [7, 26]. Finally, the Tom^{Low} population most likely does not contain bronchoalveolar stem cells (BASCs) for several reasons. First, most of the Tom^{Low} cells are located in the respiratory epithelium and do not display high levels of *Scgb1a1* (data not shown). Second, scRNA-seq data indicate that, compared to AT2 cells, BASCs express a similar level of *Sftpc* and *Fgfr2* [13], suggesting that BASCs are likely contained in the Tom^{High} population. Interestingly, lineage tracing of BASCs upon injury indicates that these cells are not the sole contributors to newly formed bronchial airway cells after conducting airway injury or AT2/AT1 cells after alveolar injury, demonstrating that other resident stem cells such as the AT2 Tom^{Low} or the AT2 could contribute to the repair process. Furthermore, PD-L1 is highly expressed in Tom^{Low}. PD-L1 expression is also increased in adenocarcinoma and appears to be correlated with elevated tumour proliferation and aggressiveness [14, 16, 25, 27, 28]. Further investigations are required to elucidate PD-L1 function in Tom^{Low} cells and their potential interaction with the immune system as well as their contribution to cancer. In the future, it will be
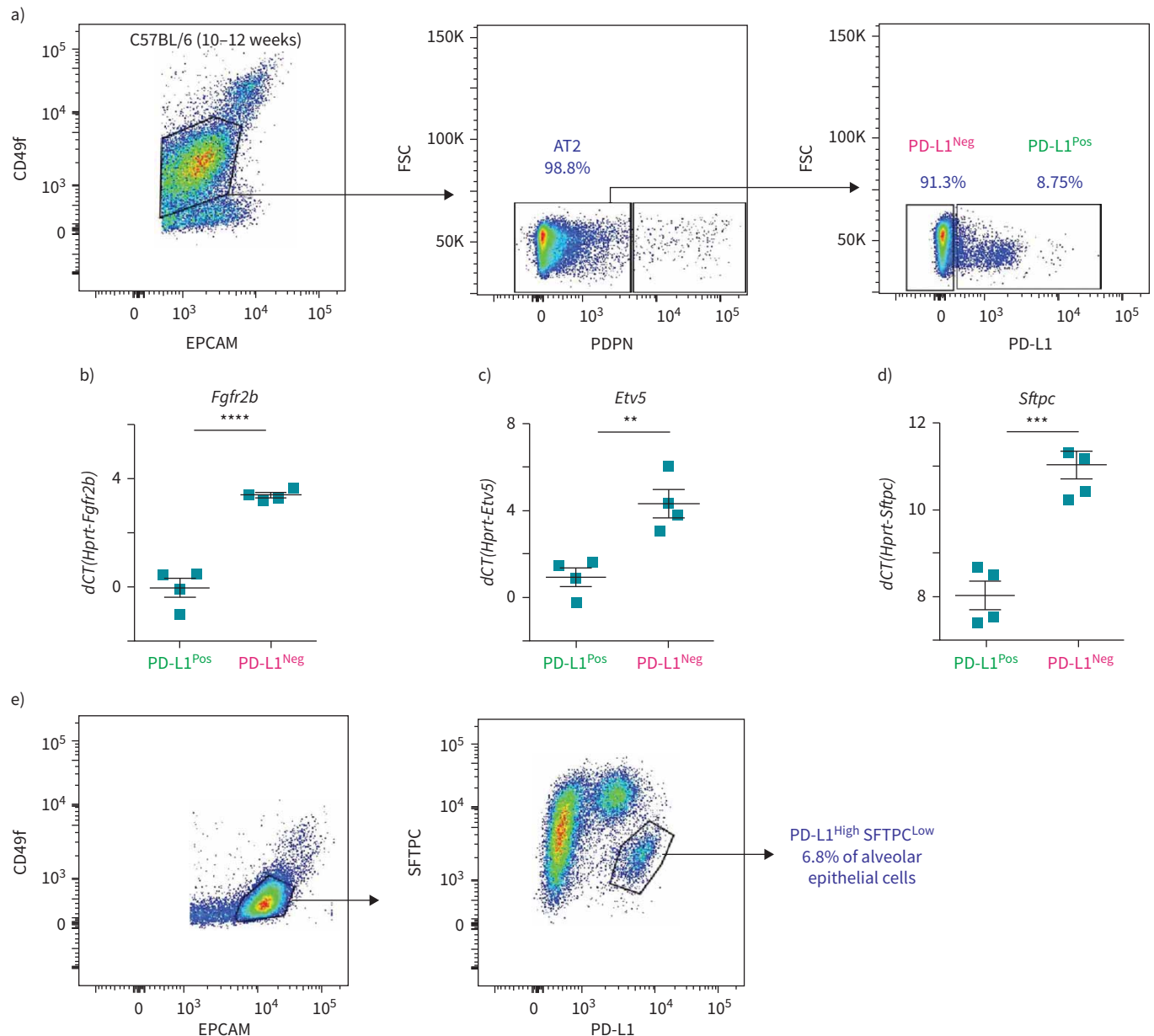
FIGURE 7 Identification of AT2 PD-L1^{Pos} cells in the lungs of wild-type mice. a) Representative flow cytometry analysis of wild-type mice lungs shows the gating strategy of EPCAM^{Pos} CD49f^{Inter} population, followed by negative selection of AT2 cells with the exclusion of AT1 PDPN^{Pos} cells. The third plot is a representative flow cytometry analysis of AT2 cells based on the use of the PD-L1 marker. b–d) Quantitative PCR analysis of fluorescence-activated cell sorting (FACS)-based sorted PD-L1^{Pos} and PD-L1^{Neg} cells for expression of *Fgfr2b* (b), *Etv5* (c) and *Sftpc* (d) (n=4). Data are presented as mean±SEM. **: p<0.01; ***: p<0.001; ****: p<0.0001. e) Representative flow cytometry analysis of SFTPC and PD-L1 co-staining. FSC: forward scatter; dCT: delta cycle threshold.

important to design dual lineage tracing strategies based on the expression of *Sftpc* and *Pd-l1* to label the Tom^{Low} cells specifically.

A scRNA-seq data set examining the status of lung cells in adult mice at different time points following bleomycin injury was recently published [29]. Data mining of these scRNA-seq results indicated that AT2 *Pd-l1*^{Pos} cells could not be detected either in control (saline) or experimental (bleomycin) conditions. Because the design of the experiment was to capture all the cells in the lung, the corresponding epithelial portion was clearly underpowered because not enough subpopulations of AT2 cells were available for a robust analysis. This lack of detection of AT2 *Pd-l1*^{Pos} cells was also likely due to the trauma associated
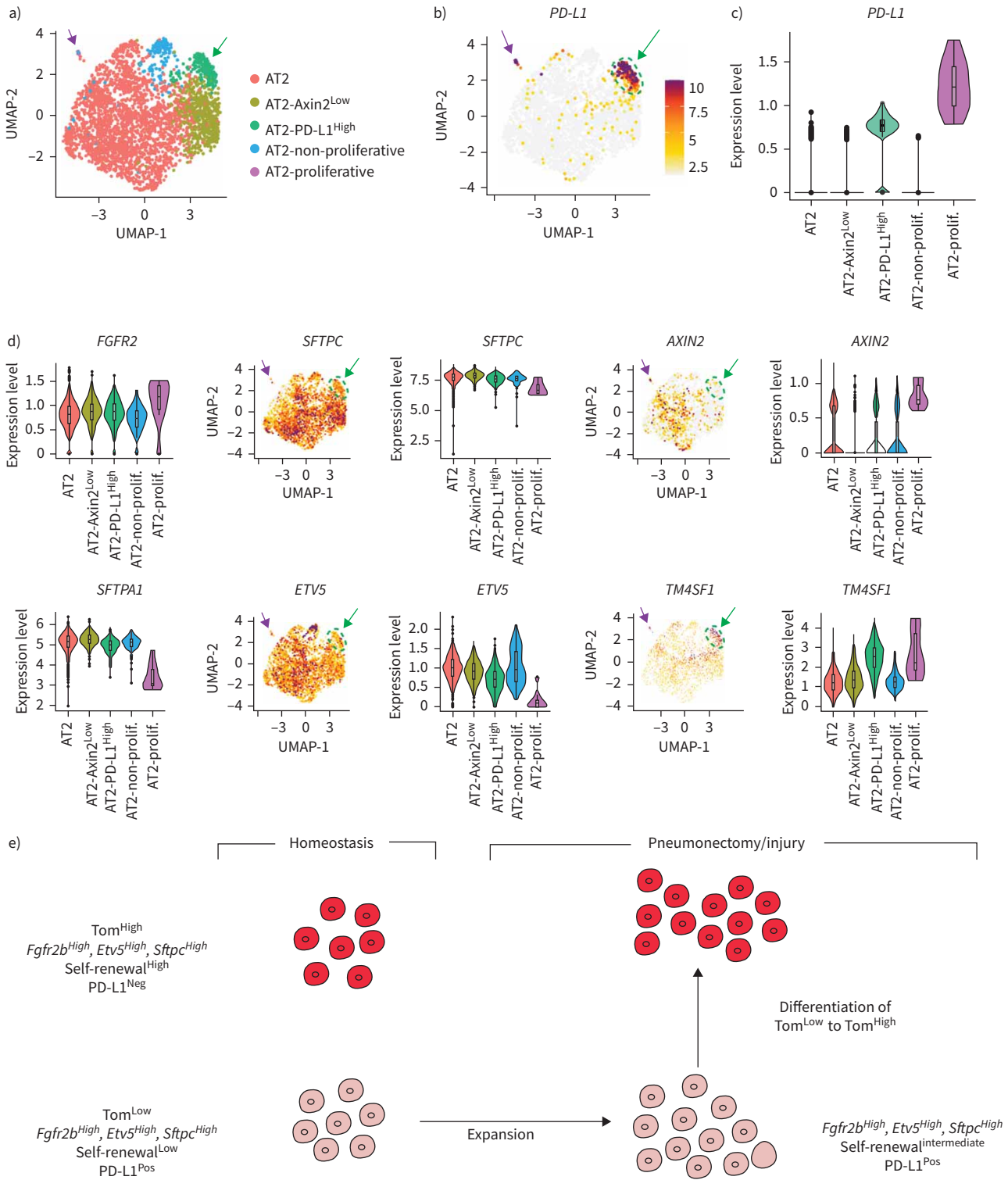
FIGURE 8 Identification of PD-L1^{Pos} cells in human AT2 single-cell RNA-sequencing (scRNA-seq) data set. a) UMAP plot of the initial AT2 cell cluster indicates the presence of five different AT2 sub-clusters. b) UMAP and c) violin plots showing *PD-L1* enrichment in the AT2-*PD-L1*^{High} sub-cluster. d) UMAP and violin plots showing that the AT2-*PD-L1*^{High} sub-cluster displays low levels of *ETV5*, *SFTPC* and *AXIN2* and high levels of *TM4SF1*. Green arrows indicate AT2 *PD-L1*^{High} and lavender arrows indicate AT2-proliferative. e) Model for tdTomato^{Low} (Tom^{Low}) and tdTomato^{High} (Tom^{High}) cells in homeostasis and after pneumonectomy/injury. Tom^{Low} cells are quiescent in the adult lung during homeostasis but are activated after injury. They acquire proliferative capabilities and differentiate into mature AT2 cells.

with the enzymatic digestion of the lung before the scRNA-seq procedure and is supported by our observation that Tom^{Low} cells had much lower viability compared to the Tom^{High} cells (data not shown). Preliminary experiments on bleomycin-treated (n=2 mice) *versus* saline-treated (n=3 mice) wild-type mice indicated a robust increase in AT2 PD-L1^{Pos} cells compared to AT2 PD-L1^{Neg} cells (21.2% *versus* 8.1%; data not shown). We, therefore, conclude that AT2 PD-L1^{Pos} (Tom^{Low}) cells appear to respond to at least three types of injury (PNX, bleomycin and PCLS).

An important question that we attempted to answer in this study is related to the potential role played by Tom^{Low} cells as progenitors for mature AT2 cells. The arguments for such a role are as follow: 1) Tom^{Low} cells represent a stable population over time (supplementary figure S4); 2) analysis of apoptosis and proliferation of the Tomato labelled cells in the PCLS model (figure 5) shows that Tom^{High} cells are massively dying while Tom^{Low} cells are proliferating; 3) there was an increase in the Tom^{Low} (PD-L1^{Pos}) pool in the context of PNX *versus* Sham (figure 4 and supplementary figure S8) without a significant change in the number of Tom^{High} cells; 4) while Tom^{Low} cells from non-injured lung indicate that these cells are not capable of self-renewal and differentiation (figure 3), our preliminary data (not shown) indicate that Tom^{Low} cells from *Sftpc$^{CreERT2/+}$;Fgfr2b$^{flox/flox}$;Tomato$^{flox/flox}$* lungs display a significant increase in alveolosphere formation, indicating that Tom^{Low} cells acquire self-renewal and differentiation capabilities.

In conclusion, we have identified a novel population of quiescent and immature AT2 progenitor cells with a different gene expression profile from mature AT2 cells that proliferate after PNX and are enriched in Pd-l1 expression. The equivalent of this population was also identified in human lungs. Further characterisation of these cells in homeostatic and repair/regeneration conditions will allow the signalling pathways activated in these cells to be identified, with the ultimate goal of enhancing repair after injury.

References

1   Fehrenbach H. Alveolar epithelial type II cell: defender of the alveolus revisited. *Respir Res* 2001; 2: 33–46.

2   Desai TJ, Brownfield DG, Krasnow MA. Alveolar progenitor and stem cells in lung development, renewal and cancer. *Nature* 2014; 507: 190–194.

3   Barkauskas CE, Cronce MJ, Rackley CR, *et al.* Type 2 alveolar cells are stem cells in adult lung. *J Clin Invest* 2013; 123: 3025–3036.

4   Rawlins EL, Okubo T, Xue Y, *et al.* The role of Scgb1a1$^+$ Clara cells in the long-term maintenance and repair of lung airway, but not alveolar, epithelium. *Cell Stem Cell* 2009; 4: 525–534.

5   Rock JR, Barkauskas CE, Cronce MJ, *et al.* Multiple stromal populations contribute to pulmonary fibrosis without evidence for epithelial to mesenchymal transition. *Proc Natl Acad Sci USA* 2011; 108: E1475–E1483.

6   Reddy R, Buckley S, Doerken M, *et al.* Isolation of a putative progenitor subpopulation of alveolar epithelial type 2 cells. *Am J Physiol Lung Cell Mol Physiol* 2004; 286: L658–L667.

7   Chapman HA, Li X, Alexander JP, *et al.* Integrin α6β4 identifies an adult distal lung epithelial population with regenerative potential in mice. *J Clin Invest* 2011; 121: 2855–2862.

8   Nabhan AN, Brownfield DG, Harbury PB, *et al.* Single-cell Wnt signaling niches maintain stemness of alveolar type 2 cells. *Science* 2018; 359: 1118–1123.

9   Zacharias WJ, Frank DB, Zepp JA, *et al.* Regeneration of the lung alveolus by an evolutionarily conserved epithelial progenitor. *Nature* 2018; 555: 251–255.

10   Frank DB, Peng T, Zepp JA, *et al.* Emergence of a wave of Wnt signaling that regulates lung alveologenesis by controlling epithelial self-renewal and differentiation. *Cell Rep* 2016; 17: 2312–2325.

11   Bender Kim CF, Jackson EL, Woolfenden AE, *et al.* Identification of bronchioalveolar stem cells in normal lung and lung cancer. *Cell* 2005; 121: 823–835.

12 Salwig I, Spitznagel B, Vazquez-Armendariz AI, *et al.* Bronchioalveolar stem cells are a main source for regeneration of distal lung epithelia *in vivo*. *EMBO J* 2019; 38: e102099.

13 Liu Q, Liu K, Cui G, *et al.* Lung regeneration by multipotent stem cells residing at the bronchioalveolar-duct junction. *Nat Genet* 2019; 51: 728–738.

14 Pawelczyk K, Piotrowska A, Ciesielska U, *et al.* Role of PD-L1 expression in non-small cell lung cancer and their prognostic significance according to clinicopathological factors and diagnostic markers. *Int J Mol Sci* 2019; 20: 824.

15 Lin G, Fan X, Zhu W, *et al.* Prognostic significance of PD-L1 expression and tumor infiltrating lymphocyte in surgically resectable non-small cell lung cancer. *Oncotarget* 2017; 8: 83986–83994.

16 Lastwika KJ, Wilson W, Li QK, *et al.* Control of PD-L1 expression by oncogenic activation of the AKT-mTOR pathway in non-small cell lung cancer. *Cancer Res* 2016; 76: 227–238.

17 Travaglini KJ, Nabhan AN, Penland L, *et al.* A molecular cell atlas of the human lung from single-cell RNA sequencing. *Nature* 2020; 587: 619–625.

18 Butler A, Hoffman P, Smibert P, *et al.* Integrating single-cell transcriptomic data across different conditions, technologies, and species. *Nat Biotechnol* 2018; 36: 411–420.

19 Hafemeister C, Satija R. Normalization and variance stabilization of single-cell RNA-seq data using regularized negative binomial regression. *Genome Biol* 2019; 20: 296.

20 Finn J, Sottoriva K, Pajcini KV, *et al.* Dlk1-mediated temporal regulation of Notch signaling is required for differentiation of alveolar type II to type I cells during repair. *Cell Rep* 2019; 26: 2942–2954.e5.

21 Leeman KT, Pessina P, Lee JH, *et al.* Mesenchymal stem cells increase alveolar differentiation in lung progenitor organoid cultures. *Sci Rep* 2019; 9: 6479.

22 Chamoto K, Gibney BC, Ackermann M, *et al.* Alveolar epithelial dynamics in postpneumonectomy lung growth. *Anat Rec (Hoboken)* 2013; 296: 495–503.

23 Lechner AJ, Driver IH, Lee J, *et al.* Recruited monocytes and type 2 immunity promote lung regeneration following pneumonectomy. *Cell Stem Cell* 2017; 21: 120–134.

24 Liu Zhe, Fu Siling, Tang Nan. A standardized method for measuring internal lung surface area *via* mouse pneumonectomy and prosthesis implantation. *J Vis Exp* 2017; 125: 56114.

25 Miyazawa T, Marushima H, Saji H, *et al.* PD-L1 expression in non-small-cell lung cancer including various adenocarcinoma subtypes. *Ann Thorac Cardiovasc Surg* 2019; 25: 1–9.

26 Vaughan AE, Brumwell AN, Xi Y, *et al.* Lineage-negative progenitors mobilize to regenerate lung epithelium after major injury. *Nature* 2015; 517: 621–625.

27 Cooper WA, Tran T, Vilain RE, *et al.* PD-L1 expression is a favorable prognostic factor in early stage non-small cell carcinoma. *Lung Cancer* 2015; 89: 181–188.

28 Yu H, Boyle TA, Zhou C, *et al.* PD-L1 expression in lung cancer. *J Thorac Oncol* 2016; 11: 964–975.

29 Strunz M, Simon LM, Ansari M, *et al.* Alveolar regeneration through a Krt8^{+} transitional stem cell state that persists in human lung fibrosis. *Nat Commun* 2020; 11: 3559.